IEEE Access
Multidisciplinary | Rapid Review | Open Access Journal

Received August 2, 2021, accepted August 17, 2021, date of publication August 19, 2021, date of current version August 26, 2021.

Digital Object Identifier 10.1109/ACCESS.2021.3106145

Model Predictive Control-Based Optimized Operation of a Hybrid Charging Station for Electric Vehicles

ENRIQUE GONZÁLEZ-RIVERA[1], PABLO GARCÍA-TRIVIÑO[1], RAÚL SARRIAS-MENA[2], JUAN P. TORREGLOSA[3], FRANCISCO JURADO[4], (Senior Member, IEEE), AND LUIS M. FERNÁNDEZ-RAMÍREZ[1], (Senior Member, IEEE)

[1]Research Group in Sustainable and Renewable Electrical Technologies (PAIDI-TEP023), Department of Electrical Engineering, Higher Technical School of Engineering of Algeciras (ETSIA), University of Cádiz, Algeciras, 11202 Cádiz, Spain
[2]Research Group in Sustainable and Renewable Electrical Technologies (PAIDI-TEP023), Department of Engineering in Automation, Electronics and Computer Architecture & Networks, University of Cádiz, Higher Technical School of Engineering of Algeciras (ETSIA), Algeciras, 11202 Cádiz, Spain
[3]Electrical Engineering Department, University of Huelva, 21071 Huelva, Spain
[4]Research Group in Research and Electrical Technology, Department of Electrical Engineering, EPS Linares, University of Jaén, 23700 Linares, Spain

Corresponding author: Luis M. Fernández-Ramírez (luis.fernandez@uca.es)

This work was supported in part by Spain's Ministerio de Ciencia, Innovación y Universidades (MCIU), Agencia Estatal de Investigación (AEI), and Fondo Europeo de Desarrollo Regional (FEDER) Unión Europea (UE) under Grant RTI2018-095720-B-C32.

ABSTRACT This paper presents an energy management system (EMS) based on a novel approach using model predictive control (MPC) for the optimized operation of power sources in a hybrid charging station for electric vehicles (EVs). The hybrid charging station is composed of a photovoltaic (PV) system, a battery, a complete hydrogen system based on a fuel cell (FC), electrolyzer (EZ), and tank as an energy storage system (ESS), grid connection, and six fast charging units, all of which are connected to a common MVDC bus through Z-source converters (ZSC). The MPC-based EMS is designed to control the power flow among the energy sources of the hybrid charging station and reduce the utilization costs of the ESS and the dependency on the grid. The viability of the EMS was proved under a long-term simulation of 25 years in Simulink, using real data for the sun irradiance and a European load profile for EVs. Furthermore, this EMS is compared with a simpler alternative that is used as a benchmark, which pursues the same objectives, although using a states-based strategy. The results prove the suitability of the EMS, achieving a lower utilization cost (-25.3%), a notable reduction in grid use (-60% approximately) and an improvement in efficiency.

INDEX TERMS Charging station, electric vehicles, energy management system, model predictive control, Z-source converters.

I. INTRODUCTION

The reduction of emissions linked to road transport is a challenge being faced all over the world. In the EU, passenger cars and vans ('light commercial vehicles') are responsible for approximately 12% and 2.5% of the total EU emissions of carbon dioxide (CO2), respectively, the main greenhouse gas. Measures and policies to reduce CO2 emissions in the transport sector have been widely addressed in the literature [1]. A relevant concern for many authors is the increase in electricity demand caused by a growing number of EVs, which could have a negative impact on the grid in terms of overcapacity. Various solutions have been proposed in the literature to constrain the rise in CO2 emissions and cater to the requirements of clean energy. The use of renewable energy, specifically PV-based energy generation, to meet the rising electricity demand for charging EVs, is a widely discussed approach [2], [3]. The difference between the PV generation and the charging profile of the EV poses a challenge for the optimal management of charging stations integrated with PV generation. To make these facilities profitable, it is important to maximize the self-consumption rate. Self-consumption can be increased by integrating energy storage systems (ESS) in the system: ESS can be charged with excess PV generation or the grid during off-peak market periods, while using the energy stored in the ESS to charge the EVs during peak periods [4].

It is clear that further research is necessary in terms of control and energy management in renewable energy-based charging stations for EVs to make them adaptable to the

The associate editor coordinating the review of this manuscript and approving it for publication was Chandan Kumar.

charging requirements. The control systems that regulate the energy exchange between the different elements in these facilities are known as energy management systems (EMS). Their design is challenging due to the variable electricity production of the PV system and the random traffic of EVs in the charging station. A review of the available literature reveals various references dealing with the EMS of fast-charging stations with PV generation and batteries as ESSs (BESSs). Rule-based and predictive controllers to deal with EMS requirements in decentralized systems were discussed in [5] and [6]. Although the utility grid support was penalized in these studies (the proposed EMSs were specifically designed to operate the charging stations mainly as stand-alone systems), both works focused on the electrical operation of the EMS while neglecting economic aspects. Simulation results showed that the fast-charging station (FCS) operated smoothly and effectively, and worked as a stand-alone system most of the time with only occasional grid support owing to its decentralized control. In [7], an adaptive fuzzy logic controller was proposed for a FC-battery hybrid power system in an EV. This controller achieved real-time control and effective power allocation.

In [8], a rule-based EMS that minimized the utility grid consumption and stores PV generation when the EVs are not being charged was proposed. The EMS was validated through model simulation in MATLAB-Simulink and laboratory-scale experimental tests. The results showed the proper regulation of the DC bus voltage under all the operation modes, including cases of overloaded utility grid, low solar irradiation, or temporarily interrupted ESS.

An EMS for an EV charging station designed as a DC microgrid was presented in [9]. A flywheel and batteries were used as the ESS in the charging station. The EMS was based on voltage droop control with hysteresis controllers to avoid frequent switching among the control modes. The EMS also used a low-pass filter that discriminated between low- and high-frequency components. Each ESS was used for a specific frequency range according to the different dynamic response of the batteries and the flywheel. The simulations showed the improvements in the hybrid ESS in the smooth transition among operation modes and the satisfactory performance of the EMS under different scenarios. Moreover, the authors highlighted the need for further improvement in the performance of the control system to ensure a reliable operation, as well as to monitor power flows for adequate management of the charging station.

As noted, the EMS presented in the aforementioned works focused on the dynamic response of the different elements of the charging station. However, these EMSs required upper layers to control the charging schedule of the EV, to predict the future production of the renewable sources, or to make decisions about the power exchange with the grid considering economic aspects. In those studies, implementing this upper layer structure, the sampling time in simulations and experiments was typically larger than that in dynamic stability studies. To validate the adequate performance of the upper control layers, simulations of several years of duration with sampling times of minutes or hours are common. These types of upper-layer EMSs often appear in microgrid studies, but they are not frequent in PV-based charging stations. In [10], the challenge posed for optimal energy management by the high inter-temporal variation of electricity production from the PV system and the variable traffic in the parking station was highlighted. To address this challenge, the authors incorporated an ESS into the charging station and provided the station with vehicle-to-grid (V2G) capability. These modifications brought complexity to the system, which required a sophisticated EMS to optimize the charge and discharge schedules of the EV and the ESS. Additionally, the EMS avoided overloading and minimized the operational cost of the station, prioritizing the use of the energy obtained from the PV system and the ESS. The novelty of this work was to employ an EMS with a valid mathematical formulation for real-time applications, since most of the previous studies used nonlinear formulation with optimization methods that could not run in real time.

Model predictive control (MPC) as an EMS in hybrid power systems combining renewable resources and ESS has been applied in several studies. In [11], a MPC-based EMS was used to regulate the SOC of an ultracapacitor. In this study, the costs of the system were not considered, and short-term operation was considered. In [12], an online distributed MPC-based optimal scheduling was applied to EV charging stations. This EMS minimized the charging station energy costs under the power flow and voltage constraints. Short-term simulations were shown. An integrated motion and powertrain modeling and control for an intelligent fuel cell/battery hybrid vehicle was proposed in [13]. A nonlinear MPC was applied to solve the integrated control problem. The authors did not consider the cost of the devices and their replacement. MPC has been applied to microgrids in different applications. However, to the best of our knowledge, no paper has been published with a similar configuration, control system implementation, and simulation length to those used in this work. A comprehensive review of MPC in microgrids with more than one hundred references has been published recently [14]. In this study, predictive control approaches were classified into three different layers in the hierarchical control of microgrids. The EMS presented herein belongs to the tertiary control layer, more specifically, to the MPC-based power management and economic optimization of microgrids. None of the works on microgrid tertiary control cited in [14] presented the same approach and objectives as the EMS presented in this paper. A model-free predictive current control of a voltage source inverter was presented in [15]. This method was based on a recursive least squares algorithm to identify the parameters of an autoregressive with exogenous input model, which provided an accurate prediction of the controlled variables. An improved finite control set-MPC for sharing power for islanded AC microgrids was proposed in [16]. This MPC strategy was applied to paralleled voltage-source inverters. The voltage tracking loop used this

MPC with a capacitor current estimator to regulate the output voltage of the voltage source inverter.

Other MPC strategies applied to microgrids with hybrid configurations have been described in [17]–[20]. In [17], MPC was used to regulate the power flow through a DC/DC converter and a voltage-source inverter of a hybrid PV/battery-based islanded AC microgrid. The input variables were the voltages and currents needed to control the converters and power flow, while the output variables were the switching pulses of the converters. A 2.5s simulation was carried out to prove the performance of the MPC. A market-oriented EMS for a hybrid power system with a wind turbine and BES was presented in [18]. In this case, the MPC used three input variables and one output variable, and it was evaluated for a 24 hours-simulation. In [19], an economic MPC-based EMS was implemented to optimize the economic dispatch of a microgrid integrating a wind turbine, a PV system, and a BES. The input variables were the electricity price, weather forecast, and energy demand, and the simulation was conducted over a week. An EMS based on MPC was presented in [20] to improve the use of renewable generation, the operational efficiency of the microgrid, and reduce the rate of degradation of storage systems. The inputs of the MPC were the ESS state, PV generation, and load, and the outputs were the power commands to the ESS converters. The results were evaluated through a simulation of a week length.

The MPC-based EMS proposed in this work fills the gap in the EMS for DC fast-charging stations, including a PV system and batteries as an ESS. Additionally, all the energy sources are connected to a common MVDC bus through ZSCs: DC/DC ZSC for PV and hydrogen systems, and a DC/AC Z-source inverter (ZSI) integrating BES for the grid connection. This type of converters presents a specific structure to achieve a large voltage buck-boost [21]. In the case of the ZSI, the impedance network between the converter and the power source allows the converter to work in a single stage, integrating the stage of the DC-DC boost and inverter into the same element. Robustness, reliability, and lower costs can be achieved by the single-stage conversion. In [22], the authors compared the ZSI with a conventional PWM inverter to highlight the advantages. On the other hand, the DC/DC ZSC can produce a desired output voltage irrespective of the input voltage because the input can be the variable voltage obtained from the PV panel, FC, or BES. Another characteristic of these converters is that they can deal with two different energy sources in the same ZSC, without an additional DC/DC converter, which is interesting for the purpose of this study. Four DC/DC converters and one voltage source inverter were used in [23], whereas in this study, as mentioned above, a solution based only on two DC/DC ZSC and one qZSI is used to integrate the same energy sources. Furthermore, the EMS designed in [23] determined the required power of each ESS by solving, through a particle swarm optimization (PSO) algorithm, an objective function based on minimizing the utilization costs of the ESS, and improving the system efficiency. In contrast, in the current work, owing to the MPC technique, in which a determined future horizon of the charging station is considered, a different and more appropriate way to control the multi-input, multi-output (MIMO) system under study in this work is achieved. The hydrogen tank level, battery SOC, grid power, and utilization cost of the ESS are used as control variables for the MIMO MPC. Moreover, to the best of our knowledge, none of the previous works ([21]–[23]) or others in the existing literature included DC/DC ZSC and ZSI in the same configuration with different energy sources and studied the system performance in a long-term simulation.

In view of the above, the main contributions of this paper are as follows: 1) A long-term study of a microgrid for a charging station based on a new configuration, with several types of ZSC and electric energy demand. 2) Implementation of a MPC-based EMS with a plant configuration based on a MIMO system with four inputs and two outputs in the MPC, an hourly sample time, and a previous online optimization based on a linear programming method. Regarding the objectives of the EMS, the novelty is that it optimizes the operational cost of the system using the concept of the net present cost (NPC), taking into account the variation in the value of money. The use of a MPC-based EMS allows its implementation in real-time controllers. 3) Calculation of the utilization costs considering the repositions of the components over 25 years.

II. HYBRID CHARGING STATION FOR EV

A hybrid charging station with six EV fast-charging units of 45 kW according to IEC 61851-1 [24] is implemented in this paper. Fig. 1 shows the components of the hybrid system. It is composed of a PV system, two ESSs, and a grid connection. The ESSs used in this hybrid system are the hydrogen system composed of a FC, an EZ, and a hydrogen tank; and a BES. All the energy sources are connected to a common MVDC bus through the ZSC. The DC/DC ZSCs are used to link the PV system and hydrogen system to the MVDC bus. The FC uses the hydrogen stored in a hydrogen tank, which is supplied from an EZ. Both the FC and EZ are

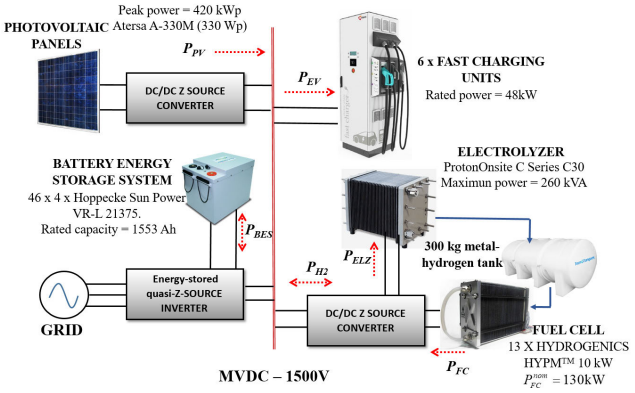

FIGURE 1. Configuration of the charging station.

connected to the same DC/DC ZSC: FC linked to the input of the ZSC and EZ in the impedance network of the ZSC. A ZSI integrating a BES into the impedance network (without an additional DC/DC converter), called energy-stored quasi-ZSI (qZSI), is used to connect the microgrid to the grid. HOMER GRID v1.2 was used for sizing the hybrid system. For the inputs of the system, a profile from the Strategy Energy Technology Plan of the EU [25] was used for the EV load, whereas the sun irradiance data were obtained from a weather station located in Algeciras (Spain).

III. MODELLING OF THE HYBRID CHARGING STATION

This section illustrates the most meaningful equations of the fast-charging station and all the components of the system for understanding the EMS. Detailed information about the model of the PV/BES/hydrogen system can be found in [26] and [27].

A. HYDROGEN SYSTEM

Thirteen 10 kW Polymer Electrolyte Membrane (PEM) FC from Hydrogenics HyPM^{TM} [28], an EZ from ProtonOnsite model C30 [29], and a 300 kg metal-hydrogen tank were used. They are connected to the common MVDC bus through a DC/DC ZSC, whose topology is described in [30]. The hydrogen level of the tank (L_{H2}) is one of the controlled parameters of the EMS. It can be calculated through an hourly flow balance between the flow of hydrogen produced and the amount of hydrogen consumed.

The maximum power that the FC and the EZ can deliver or absorb at a certain time ($P_{H2}^{max,abs}$ and $P_{H2}^{max,gen}$) is also determined by the hydrogen tank level through (1) and (2).

$$P_{H2}^{max,gen} = min\left(P_{FC}^{nom},\, U_f \cdot \eta_{them} \cdot \eta_{stack} \cdot \frac{E_{H2}^{low} \cdot L_{H2}}{\Delta t \cdot 100}\right) \quad (1)$$

$$P_{H2}^{max,abs} = min\left(P_{ELZ}^{nom},\, B \cdot q_{H2}^{nom} + A \cdot \frac{M_{H2}^{nom}}{\Delta t} \cdot \left(\frac{100 - L_{H2}}{100}\right)\right) \quad (2)$$

where P_{FC}^{nom} is the FC nominal power, U_f is the FC utilization factor, η_{them} is thermodynamic efficiency, η_{stack} is the stack efficiency, E_{H2}^{low} is the hydrogen lower calorific power, P_{ELZ}^{nom} is the EZ nominal power, A and B are the EZ constant model, and q_{H2}^{nom} is the nominal hydrogen flow of the EZ. The maximum allowed degradation, rated degradation, and warranty are related to the FC life, according to [31].

B. BATTERY ENERGY STORAGE SYSTEM

A lead-acid battery from Hoppecke^{TM} [32] is used as the BES of the charging station. The commercial model of this battery is Sun Power VR-L, which can absorb a maximum power around 3.8 kW and has a nominal capacity of 1553 Ah. In this study, it was necessary to build a configuration with 4 parallel strings of 46 batteries connected in series. This battery is integrated into an energy-stored qZSI, whose topology is described in [33], which connects the common MVDC bus of the microgrid to the grid.

The state of charge (SOC) is the first variable controlled by the EMS. It can be obtained through an hourly energy balance between the energy delivered and absorbed by the BES.

The maximum charge and discharge power of the BES (P_{BES}) in a sample period can be calculated using (3).

$$\begin{aligned} P_{BES}^{max,dis} &= min\left(P_{BES}^{nom}, \frac{E_{BES}^{nom}}{\Delta t}\left(\frac{SOC - SOC_{min}}{100}\right)\right) \\ P_{BES}^{max,char} &= min\left(P_{BES}^{nom}, \frac{E_{BES}^{nom}}{\Delta t}\left(1 - \frac{SOC}{100}\right)\right) \end{aligned} \quad (3)$$

where $P_{BES}^{max,dis}$ is the BES maximum discharge power in a sample time, P_{BES}^{nom} is the nominal power of the BES, SOC_{min} is the minimum BES SOC allowed, and $P_{BES}^{max,char}$ is the BES maximum charge power in a sample time.

The portion of nominal charging/discharging cycles completed in a sample time is another important variable of the BES. The calculation of this parameter is carried out through the BES depth-of-discharge (*DOD; DOD = 100-SOC*) [34].

C. PV SYSTEM AND ELECTRIC DEMANDS

The PV system, composed of panels from Atersa [35] with a peak power of 420 kW, represents the main energy source of the hybrid charging station. In addition, it is necessary to use 8 DC/DC ZSC of 60 kW working with a Maximum Power Point Tracking (MPPT) strategy. The DC/DC ZSC presented the same topology [30] as in the hydrogen system. The values of sun irradiance throughout one year are shown in Fig. 2a. These data were obtained from a weather station located in Algeciras (Spain) and were repeated for 25 years. This allows considering the seasonal variations of irradiation that occur throughout a year. It is assumed that the PV system works in the MPPT during the simulation. The profiles depicted in Fig. 2b are the hourly power demanded by the EV for one week. These profiles were obtained from the EU Strategy Energy Technology Plan [25] and were repeated for 25 years, scaled to the rated power of the charging station. In this case, because the weekly profiles correspond to average values, they are not affected by seasonal variations.

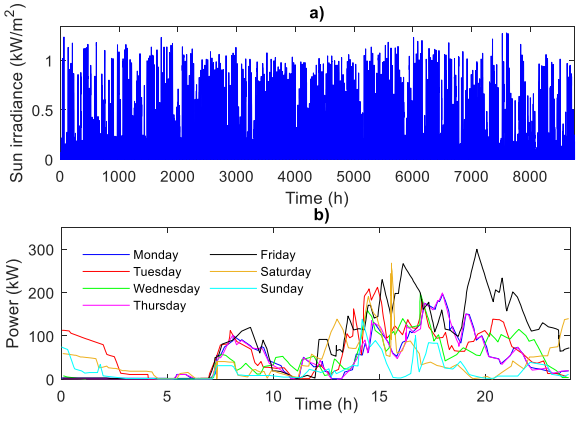

FIGURE 2. (a) Sun irradiance for one year, (b) EV power demand for one week.

D. VALIDATION OF THE MODELS

The charging station has been modeled using models widely accepted in the scientific literature. The PV panels have been modeled through the single-diode model, the BES has been taken from the SimPowerSystems Simulink toolbox, and the FC and EZ are represented by models already used and tested in similar applications (FC model in [27] and EZ model in [36]). Fig. 3 shows the validation of the models by comparing the characteristic curves obtained from the models and the real devices (real curves provided by commercial datasheets).

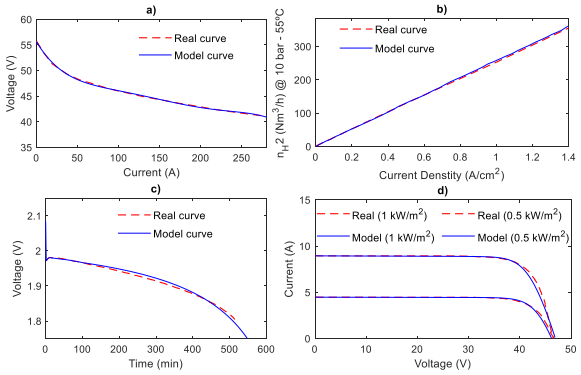

FIGURE 3. (a) FC polarization curve, (b) ELZ hydrogen production curve, (c) Battery discharge curve, and (d) PV panels current-voltage curve.

The FC has been modeled using the model already presented and verified in [27]. The voltage-current curve obtained from the model and the curve of the commercial FC are shown in Fig. 3a. The EZ has been modelled according to the model B developed in [36]. Fig. 3b illustrates the hydrogen production obtained from the real EZ and from the model. Fig. 3c shows the battery discharge curve (voltage versus time) obtained from the model and from the real battery. Finally, the current-voltage curves of the PV panels for 1000 W/m^2 and 500 W/m^2 are illustrated in Fig. 3d.

As it can be seen, the results reflect an accurate approximation of the models to the performance of the real devices.

IV. OPTIMIZED LONG-TERM EMS FOR THE CHARGING STATION

Hybrid systems with different power sources and ESSs are usually supported by an EMS that generates the required active power references to manage energy efficiently. The proper operation of the hybrid charging station is measured in terms of the utilization cost of its elements. The primary energy source of the hybrid charging station used in this study is the PV system. The net power (P_{net}) is defined as the difference between the EV and PV power (namely P_{EV} and P_{PV}, respectively). The EMS uses P_{net} at hourly intervals to make decisions and ensure the power balance in the charging station. The EMS can make the following decisions: 1) to store the excess of renewable energy in the hydrogen tank using the EZ, or to store it in the BES; 2) to provide the power demanded by the EV through the BES or through the hydrogen system (converting the hydrogen of the tank into electricity in the FC) when the PV system cannot fulfill the

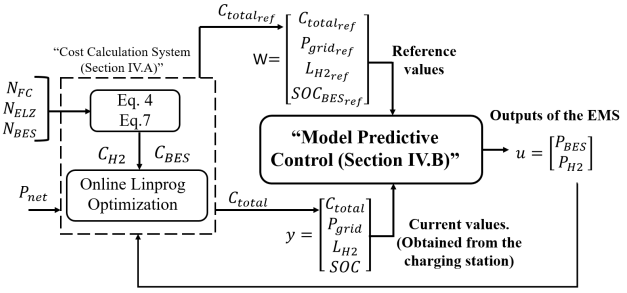

FIGURE 4. General scheme of the proposed EMS for the hybrid charging station.

EV requirements; and 3) to calculate the amount of power that must be generated or stored in a time interval. When the demanded power is not covered by the devices of the charging station, the grid contributes.

The main objective of the EMS is to minimize the utilization cost of each component considering their efficiency. To achieve this goal, the EMS is structured in two subsystems (Fig. 4): 1) a "cost calculation system" (section IV.A), which calculates the minimum utilization costs of each device taking into account P_{net} at each time interval and the reference for the total costs of the system; and 2) an "optimization algorithm" (section IV.B), which defines the optimum operating point of each device observing the BES SOC and the hydrogen tank level, and generating the output power of each component to ensure the optimum utilization cost of the hybrid charging station. The EMS obtains the average hourly values of power in both ESSs.

A. COST CALCULATION SYSTEM

This section presents the calculation of the utilization costs for each device. Additionally, to improve the performance of the EMS, it is necessary to estimate the optimum costs to use them as a reference for the MPC.

First, the utilization costs are calculated as the fraction between the costs associated with a device in a year and the expected energy to be delivered or absorbed in that year. Thus, the numerators of (4) correspond to the amount of money (net present cost, NPC) that has to be spent on a certain component (acquisition and operation and maintenance, O&M) throughout the 25 years and converted to a yearly cost by means of the SPWF. However, the denominators are related to the energy terms. Hence, in the case of the BES, this term is the energy that the BES can provide in a year. For the hydrogen system, this term is the sum of the energy that the FC can generate in a year and the energy that the ELZ can absorb in a year.

$$C_{BES}(t) = \frac{\left(NPC_{BES} + NPC_{BES}^{OM}\right)/SPWF}{E_{BES}^{cycle} \cdot N_{BES}^{eq}}$$
$$C_{H2}(t) = \frac{\left(NPC_{FC} + NPC_{FC}^{OM} + NPC_{ELZ} + NPC_{ELZ}^{OM}\right)/SPWF}{P_{FC}^{max} \cdot N_{FC}^{eq} + P_{ELZ}^{max} \cdot N_{ELZ}^{eq}} \quad (4)$$

where $C_i(t)$ is the utilization cost of the device, NPC_i is the NPC of the device, NPC_i^{OM} is the NPC of the O&M of the device, E_{BES}^{cycle} is the cycle energy of the BES, N_i^{eq} is the equivalent number of cycles of the BES for one year (hours in the case of the FC or ELZ), P_i^{max} is the maximum power of the device. Additionally, NPC and NPC^{OM} are obtained using (5)–(6).

$$NPC_i = Ac_i \left(\sum_{t=1}^{t=year} (1+I)^{-t} + \sum_{t=\text{year}}^{t=25} (1+I)^{t} \right) \quad with\ t = 1, 2L_i, 3L_i \ldots \tag{5}$$

$$NPC_i^{OM} = OM_i N_i^{eq} \left(\sum_{t=1}^{t=year} (1+I)^{-t} + \sum_{t=\text{year}}^{t=25} (1+I)^{t} \right) \tag{6}$$

where Ac_i is the acquisition cost, OM_i is the O&M cost, and L_i is the lifespan of each energy source.

Note that, in a certain year of the simulation, the acquisition costs of the past and future replacements throughout 25 years are considered in the first and the second terms in (5), and updated to the current year using the annual interest rate I. The O&M costs are also considered throughout 25 years, in this case, with an annual update (6).

The total cost of the system (C_{total}) is calculated using (7). As explained in the next section, the EMS generates a solution for the objective function to minimize the utilization cost of the hybrid charging station (€/h) in each sample time. The grid connection must be avoided whenever possible.

$$C_{total} = C_{BES} \cdot P_{BES} + C_{H2} \cdot P_{H2} + \left[\max\left(C_{BES}, C_{H2}\right) \cdot P_{grid,ex} \right] \tag{7}$$

where $P_{grid,ex}$ is the power exchanged between the system and the grid.

It should be noted that the EMS tries to avoid or limit the use of the grid. To achieve this objective, the maximum value between C_{BES} and C_{H2} is multiplied by $P_{grid,ex}$ This term works as a penalty for not using the other energy sources (BES of hydrogen system).

Additionally, as previously mentioned, optimization of the reference costs for the MPC is carried out to improve the performance of the system. This optimization is solved using the linear programming method [37], as shown in (8):

$$\min f^T\ x\ such\ that \begin{cases} A \cdot x \leq b \\ Aeq \cdot x = beq \\ lb \leq x \leq ub \end{cases} \tag{8}$$

The cost function is defined by (9). This function must comply with (10) and the restrictions in (11).

$$C_{total}^{ref} = C_{BES} \cdot P_{BES} + C_{H2} \cdot P_{H2} \tag{9}$$

$$C_{BES} \cdot P_{BES} + C_{H2} \cdot P_{H2} = P_{net} \tag{10}$$

$$-P_{BES}^{max} \leq P_{BES} \leq P_{BES}^{max}$$
$$-P_{ELZ}^{max} \leq P_{H2} \leq P_{FC}^{max} \tag{11}$$

where the power limits of the BES are denoted as $-P_{BES}^{max}$ (maximum discharging power) and P_{BES}^{max} (maximum charging power), and the power limits of the hydrogen system are denoted as $-P_{ELZ}^{max}$ (maximum power absorbed by the EZ) and P_{FC}^{max} (maximum power generated by the FC).

Note that this optimization is carried out in each sample time. Therefore, this is an online optimization algorithm. The results obtained here are inputted to the MPC, which minimizes the difference between the reference costs, calculated using (9)–(11), and the real costs measured each sample time.

B. OPTIMIZATION PROBLEM: MODEL PREDICTIVE CONTROL

MPC is a widely used control strategy because of being an optimization technique. It is based on the prediction of the state of the system in a determined future horizon [38]. The optimization is performed over the prediction horizon by minimizing a cost function.

A trajectory of the control output is defined by the optimization algorithm. This trajectory achieves an adequate reference tracking of the output. Generating a linear time-invariant (LTI) model of the system is mandatory. The Simulink Control Design toolbox was used for this purpose. The MPC algorithm uses the resulting LTI model, system output, and control signal to infer the evolution of the system. Quadratic programming (QP) is used by the MPC algorithm to solve the optimization problem at each control interval [39]. After solving the optimization problem, the MPC defines the manipulated variable, which is inputted to the system during a control interval.

In this case, a MIMO LTI model of the system is needed, because the MPC has to deal with multiple variables. The inputs of the MPC block (Fig. 4) are the BES SOC with its reference, the hydrogen tank level with its reference, $P_{grid,ex}$ with its reference, and the total costs of the devices with their references. In contrast, the BES power and hydrogen system power are the outputs of the MPC block. The theoretical cost function (J) for a MIMO system is given by (12):

$$J = \sum_{i=1}^{P_H} \| y(k+i|k) - W(k+i|k) \|^2 Q_1 + \sum_{i=1}^{N} \| \Delta u(k+i-1|k) \|^2 Q_2 \tag{12}$$

where P_H is the prediction horizon, $y(k+i|k)$ is the predicted output variable at the ith prediction horizon step, $W(k+i|k)$ is the reference value at the ith prediction horizon step, $u(k+i|k)$ is the control action at the ith prediction horizon step, N is the control horizon, and the terms Q_1 and Q_2 are weight matrixes.

Note that the other terms in (12) are matrixes as well. Additionally, the decision delivered by the QP is given by (13).

$$y = \begin{bmatrix} y(k|k) \\ y(k+1|k) \\ \vdots \\ y(k+P-1|k) \end{bmatrix} u = \begin{bmatrix} u(k|k) \\ u(k+1|k) \\ \vdots \\ u(k+N-1|k) \end{bmatrix} \tag{13}$$

Eq. (14) shows the elements of the MIMO system.

$$y = \begin{bmatrix} SOC_{BES} \\ L_{H2} \\ P_{grid,ex} \\ C_{total} \end{bmatrix} \quad W = \begin{bmatrix} SOC_{BES}^{ref} \\ L_{H2}^{ref} \\ P_{grid,ex}^{ref} \\ C_{total}^{ref} \end{bmatrix} \quad u = \begin{bmatrix} P_{BES} \\ P_{H2} \end{bmatrix}$$
$$Q_1 = \begin{bmatrix} \delta_1 & 0 & 0 & 0 \\ 0 & \delta_2 & 0 & 0 \\ 0 & 0 & \delta_3 & 0 \\ 0 & 0 & 0 & \delta_4 \end{bmatrix} \quad Q_2 = \begin{bmatrix} \lambda_1 & 0 \\ 0 & \lambda_2 \end{bmatrix} \quad (14)$$

where SOC_{BES}^{ref} is the reference BES SOC, L_{H2}^{ref} is the reference level of the hydrogen tank, $P_{grid,ex}^{ref}$ is the reference of $P_{grid,ex}$, C_{total}^{ref} is the reference of the total cost of the system, δ is the weight that penalizes the deviation from the output reference, and λ is the weight that penalizes the increases in the measured variable.

The reference values of vector W are defined to obtain the best performance of the entire system. For the battery, the reference SOC is set to 65%, which is the middle value between the SOC limits recommended by the manufacturer (30%–100% [29]). The reference level for the hydrogen tank (50%) is also chosen as an intermediate value between the level limits (5%–100%). On the other hand, the reference $P_{grid,ex}$, is set to zero because one of the main objectives of this work is to avoid consuming power from the grid whenever possible. Finally, the reference for the total cost of the system is calculated using the linear programming method described in Section IV.A.

In addition, it is necessary to consider certain constraints in the MPC to maintain the inputs and outputs of the system between their operating limits. As measured output constraints, the BES SOC is limited between 30% and 100% to prevent the complete discharge of the device, which could reduce its lifetime. The level of the hydrogen tank is limited between 5% and 100% to avoid complete depletion due to the safety margin of the device. The parameters and constraints of the implemented MPC are summarized in Table 1.

The weight factors have been selected following the guide on Predictive Control available in [39], and carrying out several performance tests under different weight factors. The weight factors are divided into five groups in [39]: low priority (weight factor around 0.05), below-average priority (weight factor around 0.2), average priority (weight factor around 1), above average priority (weight factor around 5), and high priority (weight factor around 20).

In this study, only three priority levels are considered, as there are only three groups of elements that require priority-level assignment. Hence, the reference weight factors suggested in [36] have been adapted to this scenario. In this sense, low priority (large tracking error acceptable) is given a value of 0.01 for the BES SOC and the hydrogen tank level. As the focus is put on the adequate power exchange among the ESS and the rest of the devices in the charging station, rather than on pursuing a specific BES SOC or hydrogen tank level, an aggressive reference tracking is not needed for these parameters. Therefore, a low priority will allow a certain regulation of the BES SOC and hydrogen tank level without being a stiff limitation for the system. On the other hand, high priority (small tracking error desired) was assigned to the reference $P_{grid,ex}$ with a weight factor of 10, which is more conservative than the value proposed in [39]. Nevertheless, it was enough for the purpose of avoiding the use of the grid whenever it was possible. Finally, an average priority was chosen for the total cost of the system because quite satisfactory results could be achieved with this priority, as the results did not differ much from the optimal ones, defined by W. This average priority was set to 1 in [39], which was checked suitable for the purpose of this work. Therefore, the highest priority in the weight factors was given to the option of avoiding the use of the grid, followed by the option of achieving the optimal total cost of the system (average priority), and finally, achieving the reference values for the BES SOC and hydrogen tank level (low priority).

TABLE 1. MPC parameters.

Controller parameters		
Control interval (h)		1
Prediction horizon (intervals)		10
Control horizon (intervals)		2
Output weights		
SOC_{BES}		0.1
L_{H2}		0.1
P_{grid}		10
C_{total}		1
Input rate weights		
P_{BES}		0.01
P_{H2}		0.01
Constraints		
Parameter	Type	Range
SOC_{BES} (%)	Level limitation	[30,100]
L_{H2} (%)	Level limitation	[5,100]

Finally, the power balance of the system is ensured through (15), where P_{gen} is the total power generated by the charging station excluding the grid, P_{PV} is the PV panel power, and P_{EV} is the EV power and $P_{grid,ex}$.

$$P_{BES}+P_{H2}+P_{grid}+P_{PV} = P_{EV}P_{gen}+P_{grid} = P_{EV} \quad (15)$$

V. RESULTS AND DISCUSSION

A 25 years-long simulation is performed to evaluate the performance of the hybrid fast charging station controlled by the predictive EMS presented in this paper. A states-based EMS is used to compare the results obtained. This EMS is described in Appendix. The data shown in Fig. 2 (i.e., the sun irradiance in Fig. 2a and the EV power demand in Fig. 2b) were repeated to obtain the 25 years simulation data, which is the expected lifespan of the hybrid charging station.

The BES and hydrogen system power of the MPC-based EMS are shown in Fig. 5a and 5b throughout the entire simulation. The generated power corresponds to the positive values in the plot, whereas the absorbed power corresponds to the negative values. In Fig. 5c, the PV system power, together

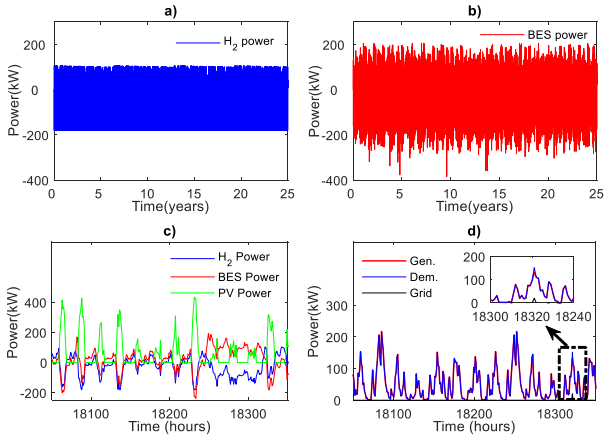

FIGURE 5. MPC-based EMS. (a) Hydrogen system power for 25 years; (b) BES power for 25 years; (c) Hydrogen system, BES and PV system power for ten days; and (d) demanded, generated power and grid power for ten days.

with the BES and the hydrogen system power, are shown in a ten-day window zoom. As shown in Fig. 5c, the BES, the hydrogen system, or both, are able to absorb or deliver the lack or excess of power from the PV system and the load demand in the EV fast charging station. Nevertheless, sometimes, they cannot supply the power demanded by the six fast-charging units. To fulfill this power shortage, the grid must inject power into the system. Fig. 5d shows the grid supporting the system to provide the power demanded by the charging station. In this situation, the PV power is null due to night-time, the BES SOC is at 30,14%, and the hydrogen tank level is 5,9%, thus being near their minimum values. Therefore, they cannot deliver more power to the EV, so they cannot address the demand completely. Because of this, there is a lack of 37,5 kW at hour 18320, which is provided by the grid.

The hydrogen tank level and the BES SOC for the MPC-based EMS are shown in Fig. 6a for the 25 years of the simulation. Note that the EMS can control both variables perfectly. The BES SOC minimum limit is fixed at 30%,

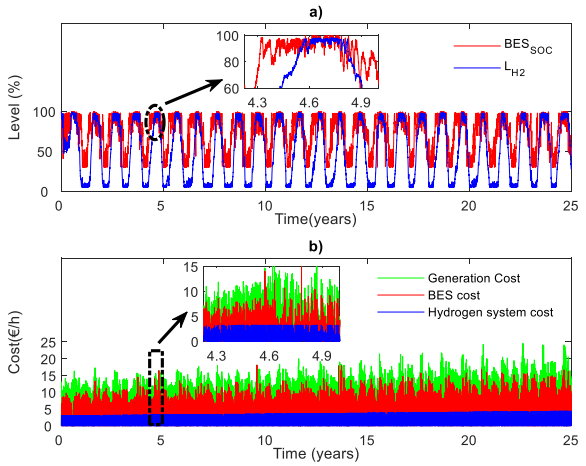

FIGURE 6. MPC-based EMS. (a) BES SOC and hydrogen tank level for 25 years; and (b) BES, hydrogen system and generation costs (€/h) for 25 years.

which implies a maximum DOD of 70%, smaller than the 80% that is the minimum level recommended by the manufacturer [32]. On the other hand, the minimum level of the hydrogen tank is set at 5% to prevent its full discharge due to the safety margin of the device. In addition, Fig. 6a shows the behavior of the hydrogen tank level and the BES SOC in a six-month zoom, where it can be seen that the controller works successfully. Fig. 6b shows the BES, the hydrogen system, and the generation cost, which is the total cost of the system, including the penalization of being supported by the grid. There is also a six-month zoom in Fig. 6b, which illustrates the management of the costs in the MPC-based EMS. The power of the BES and the hydrogen system with the state-based EMS are shown in Fig. 7a throughout the 25 years-long simulation. As previously mentioned, the generated power corresponds to positive values in the plot, whereas the absorbed power corresponds to negative values. The hydrogen tank level and the BES SOC for the state-based EMS are shown in Fig. 7b for the entire simulation. It can be seen that the hydrogen system is not working well, because the hydrogen tank is rarely full in the entire simulation.

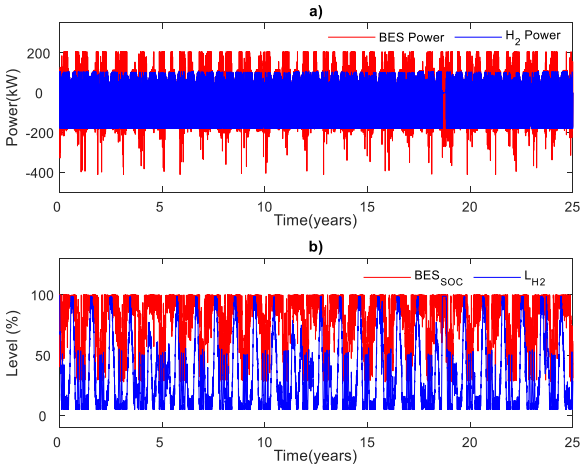

FIGURE 7. State-based EMS. (a) Hydrogen system power and BES power for 25 years; and (b) BES SOC and hydrogen tank level for 25 years.

A comparison between the MPC-based EMS and the state-based EMS is also carried out. Fig. 8a shows $P_{grid,ex}$ for both EMSs. Positive values correspond to the power injected by the grid, and negative values correspond to the power absorbed by the grid. Fig. 8a also shows a ten-day window of the previous plot, in which a better performance of the MPC-based EMS compared to the state-based system can be seen. Fig. 8b shows the costs of both EMSs in the same ten-day window. It can be observed that the costs of the MPC-based EMS are always lower than those of the state-based EMS. Therefore, it can be highlighted that the MPC-based EMS has notorious advantages compared to the state-based EMS used as a benchmark.

Additionally, Table 2 summarizes the main variables used for the comparison of both EMSs. The power delivered by the grid, the average utilization costs of both ESSs, the cost of the hybrid charging station, the efficiency of the devices,

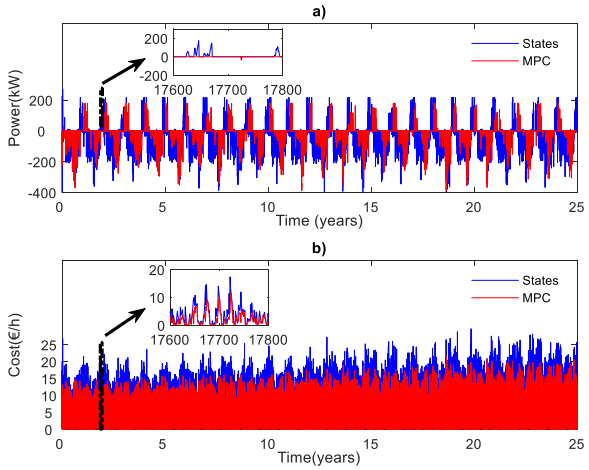

FIGURE 8. Comparison between the EMSs evaluated. (a) Power exchanged by the grid with both EMSs in 25 years; and (b) Total costs of the charging station in both EMSs in a ten-days window.

TABLE 2. Results of the comparative study.

Parameter	Proposed EMS (MPC)	Ref. EMS (States)
Power injected by the grid (MWh)	196,4 (-58,49%)	473,1
Power absorbed by the grid (MWh)	448,7 (-68,42%)	1420,7
Average utilization cost of the BES (c€/kWh)	49,547 (+0,01%)	49,542
Average utilization cost of the Hydrogen system (c€/kWh)	20,346 (+0,01%)	20,342
Total utilization cost of the hybrid charging station (€)	7,99E+6 (-25,33%)	1,07E+07
Average utilization cost of the hybrid charging station (c€/kWh)	76,74 (-27,73%)	106,18
Hourly cost of the hybrid charging station (€/h)	38,69 (-21,27%)	49,14
Efficiency of the ESS (%)	78,3 (+21,96%)	64.2
Efficiency of the charging station (%)	86,67 (+10,25%)	78,61
Average efficiency of the FC (%)	55,9% (+40,10%)	39,9
Loss of power supply probability (%)	1,85% (-58,43%)	4,45%

and the Loss of Power Supply Probability (LPSP) are shown in this table. The BES and the hydrogen system average utilization costs are slightly higher in the proposed EMS because of the time that the devices have been working. In the state-based EMS, the grid has injected more power into the hybrid system than in the MPC-based system. Subsequently, it can be expected that the average utilization costs of the ESS are lower, because of the reduced operating time. Therefore, as shown in Table 2, the generation cost (ESS utilization costs plus grid cost) is a better way to compare both EMSs.

On the other hand, the efficiencies in the MPC-based EMS are higher than those in the state-based EMS, which means that the EMS presented in this paper enhances the performance of the elements in the hybrid system. In the proposed EMS, the increase in the efficiency is 21,96% higher for the ESS, and 10,25% higher for the charging station, compared with the base case. This increase in efficiency is also reflected in the probability of unsatisfied power by the energy sources of the hybrid charging station (without considering the grid), denoted as LPSP, which is calculated using (16).

$$LPSP = \left(1 - E_{ESS}^{gen} + E_{PV}/E_{EV}\right) 100 \tag{16}$$

where E_{ESS}^{gen} is the energy generated by the ESS, E_{PV} is the energy generated by the PV panels, and E_{EV} is the energy consumed by the EV. This expression gives an idea about the percentage of energy demanded by the EV that was not generated by the ESS or the PV system. It can be noticed that owing to the better efficiency of the charging station with the proposed EMS, the LPSP is 58,43% better than with the reference EMS.

VI. CONCLUSION

A novel EMS applied to a renewable charging station for EVs was presented in this paper. Three main contributions were presented in this paper: 1) design of the hybrid system based on ZSC; 2) development of an EMS able to optimize the costs of the system throughout long-term simulations; and 3) methodology based on calculating the utilization costs of each device, including the lifespan. The EMS had also a novel structure, which was composed by: 1) a ''cost calculation system''; 2) an ''optimization algorithm'' based on MPC to make the ESS work near the optimum operation point. The results of the long-term simulations (25 years) were satisfactory. The results illustrated that the proposed EMS achieved a good compromise between the utilization cost of the hybrid charging station and the efficiency of the components. Additionally, the correct performance of the proposed EMS was verified throughout the simulation period. A comparison between the proposed EMS and a simpler EMS (state-based EMS defined in Table 3) based on states was performed. A general decrease in the cost of the proposed EMS was achieved. It is remarkable that the total cost of the hybrid charging station was significantly decreased (-25,33%), which was the main objective. Finally, better efficiencies were obtained, which resulted in a decrease in the LPSP (-58,43%).

APPENDIX EMS BASED ON STATES

The EMS based on states calculates the power commands to the BES and the hydrogen system from three variables: P_{net}, SOC, and L_{H2}.

For both the BES and hydrogen systems, two hysteresis cycles are used to classify their storage levels. Depending on the current value of the BES SOC/hydrogen tank level, the hysteresis cycles determine the state of the storage system level among the following: Low, Normal and High.

Apart from that, for both the BES and the hydrogen system, some calculations are carried out to determine their power limits. On the one hand, the maximum powers that they can generate/store depending on their current percentage of storage level are calculated. The power needed to reach the reference value of the BES SOC/hydrogen tank level from their current values are calculated as follows: 1) if the storage level is above the reference value and the system is operating under a surplus of energy ($P_{net} > 0$), this power is calculated as the power generated during one sample interval would reduce the storage level from the current value to the reference value; 2) if the storage level is below the reference value and

TABLE 3. EMS based on states (18 states).

P_{net}>0 (excess of energy)
State 1 (SOC=H, H2 level=H) $P_{BES} = \min\left(P_{BES}^{max}, P_{net}\right)$, $P_{H2} = \min\left(P_{H2}^{max}, P_{net} - P_{BES}\right)$
State 2 (SOC=H, H2 level=N) $P_{BES} = \min\left(P_{BES}^{max}, P_{net}\right)$, $P_{H2} = \min\left(P_{H2}^{max}, P_{net} - P_{BES}\right)$
State 3 (SOC=H, H2 level=L) $P_{BES} = \min\left(P_{BES,ref}^{max}, 1.2 \cdot P_{net}\right)$ If $P_{net} \geq P_{BES,ref}^{max}$, $P_{H2} = 0$; Else $P_{H2} = \max\left(P_{H2}^{min}, P_{net} - P_{BES}\right)$
State 4 (SOC=N, H2 level=H) $P_{H2} = \min\left(P_{H2}^{max}, P_{net}\right)$, $P_{bat} = \min\left(P_{BES}^{max}, P_{net} - P_{H2}\right)$
State 5 (SOC=N, H2 level=N) If $P_{net} \leq 2P_{H2}^{max}$,$P_{BES} = \min\left(P_{BES}^{max}, P_{net}/2\right)$,$P_{H2} = \min\left(P_{H2}^{max}, P_{net} - P_{BES}\right)$ Else $P_{H2} = \min\left(P_{H2}^{max}, P_{net}\right)$, $P_{bat} = \min\left(P_{BES}^{max}, P_{net} - P_{H2}\right)$
State 6 (SOC=N, H2 level=L $P_{bat} = \min\left(P_{BES}^{max}, P_{net}\right)$, $P_{H2} = 0$
State 7 (SOC=L H2 level=H) $P_{H2} = \min\left(1.2 \cdot P_{net}, P_{H2,ref}^{max}\right)$ If $P_{net} \geq P_{H2,ref}^{max}$, $P_{BES} = 0$; Else $P_{BES} = \max\left(P_{BES}^{min}, P_{net} - P_{H2}\right)$
State 8 (SOC=L, H2 level=N) $P_{H2} = \min\left(P_{H2}^{max}, P_{net}\right)$, $P_{bat} = 0$
State 9 (SOC=L, H2 level=L) $P_{bat} = 0$, $P_{H2} = 0$
P_{net}<=0 (surplus of energy)
State 10 (SOC=H, H2 level=H) $P_{BES} = P_{BES,ref}^{min}$, $P_{H2} = P_{H2,ref}^{min}$
State 11 (SOC=H, H2 level=N) $P_{H2} = \max\left(P_{net}, P_{H2}^{min}\right)$, $P_{BES} = \max\left(P_{BES}^{min}, P_{net} - P_{H2}\right)$
State 12 (SOC=H, H2 level=L) $P_{H2} = \max\left(P_{H2}^{min}, 1.2 \cdot P_{net}\right)$ If $P_{net} \leq P_{H2}^{min}$, $P_{BES} = 0$; Else $P_{BES} = \max\left(P_{BES}^{min}, P_{net} - P_{H2}\right)$
State 13 (SOC=N, H2 level=H) $P_{BES} = \max\left(P_{BES}^{min}, P_{net}\right)$, $P_{H2} = \max\left(P_{H2}^{min}, P_{net} - P_{BES}\right)$
State 14 (SOC=N H2 level=N) If $P_{net} \geq 2P_{bat\_min}$, $P_{BES} = \max\left(P_{BES}^{min}, P_{net}/2\right)$, $P_{H2} = \max\left(P_{H2}^{min}, P_{net} - P_{BES}\right)$ Else $P_{BES} = \max\left(P_{BES}^{min}, P_{net}\right)$, $P_{H2} = \max\left(P_{H2}^{min}, P_{net} - P_{BES}\right)$
State 15 (SOC=N, H2 level=L) $P_{H2} = \max\left(P_{net}, P_{H2}^{min}\right)$, $P_{BES} = \max\left(P_{BES}^{min}, P_{net} - P_{H2}\right)$
State 16 (SOC=L, H2 level=H) $P_{BES} = \max\left(P_{BES}^{min}, 1.2 \cdot P_{net}\right)$ If $P_{bat} \leq P_{BES}^{min}$, $P_{H2} = 0$; Else $P_{H2} = \max\left(P_{H2}^{min}, P_{net} - P_{BES}\right)$
State 17 (SOC=L, H2 level=N) $P_{BES} = \max\left(P_{BES}^{min}, P_{net}\right)$, $P_{H2} = \max\left(P_{H2}^{min}, P_{net} - P_{BES}\right)$
State 18 (SOC=L, H2 level=L) If $P_{net} \geq 2P_{BES}^{min}$, $P_{BES} = \max\left(P_{BES}^{min}, P_{net}/2\right)$,$P_{H2} = \max\left(P_{H2}^{min}, P_{net} - P_{BES}\right)$ Else $P_{H2} = \max\left(P_{H2}^{min}, P_{net}\right)$, $P_{BES} = \max\left(P_{BES}^{min}, P_{net} - P_{H2}\right)$

the system is operating under an excess of energy ($P_{net} \leq 0$), this power is calculated as the power that is absorbed during one sample interval would increase the storage level from the current value to the reference value; 3) in the rest of the cases, this power is equal to zero. These power limits are denoted as follows: when the system is operating under a surplus of energy ($P_{net} > 0$), $P_{BES,ref}^{max}$, and $P_{H2,ref}^{max}$ for the BES and the hydrogen system, respectively; when the system is operating under an excess of energy ($P_{net} \leq 0$), $P_{BES,ref}^{min}$ and $P_{H2,ref}^{min}$ for the BES, and the hydrogen system, respectively. Considering the storage levels, the maximum power limits according to the storage levels and the power needed to reach the reference values of the ESS, together with P_{net} of the system, the EMS composed of 18 states determines P_{BES} and P_{H2}. Table 3 lists the 18 states of this EMS.

REFERENCES

[1] D. P. Đorđe, R. P. Dalibor, M. P. Maja, and M. M. Radomir, "Electric cars: Are they solution to reduce CO_2 emission," *Thermal Sci.*, vol. 24, no. 5, pp. 2879–2889, 2020.

[2] G. R. C. Mouli, M. Kefayati, R. Baldick, and P. Bauer, "Integrated PV charging of EV fleet based on energy prices, V2G, and offer of reserves," *IEEE Trans. Smart Grid*, vol. 10, no. 2, pp. 1313–1325, Mar. 2019.

[3] A. Esfandyari, B. Norton, M. Conlon, and S. J. McCormack, "Performance of a campus photovoltaic electric vehicle charging station in a temperate climate," *Sol. Energy*, vol. 177, pp. 762–771, Jan. 2019.

[4] R. Fachrizal and J. Munkhammar, "Improved photovoltaic self-consumption in residential buildings with distributed and centralized smart charging of electric vehicles," *Energies*, vol. 13, no. 5, p. 1153, Mar. 2020.

[5] J. P. Torreglosa, P. García-Triviño, L. M. Fernández-Ramirez, and F. Jurado, "Decentralized energy management strategy based on predictive controllers for a medium voltage direct current photovoltaic electric vehicle charging station," *Energy Convers. Manage.*, vol. 108, pp. 1–13, Jan. 2016.

[6] P. García-Triviño, J. P. Torreglosa, L. M. Fernández-Ramírez, and F. Jurado, "Control and operation of power sources in a medium-voltage direct-current microgrid for an electric vehicle fast charging station with a photovoltaic and a battery energy storage system," *Energy*, vol. 115, pp. 38–48, Nov. 2016.

[7] J. Chen, C. Xu, C. Wu, and W. Xu, "Adaptive fuzzy logic control of fuel-cell-battery hybrid systems for electric vehicles," *IEEE Trans. Ind. Informat.*, vol. 14, no. 1, pp. 292–300, Jan. 2018.

[8] D. A. Savio, V. A. Juliet, B. Chokkalingam, S. Padmanaban, J. B. Holm-Nielsen, and F. Blaabjerg, "Photovoltaic integrated hybrid microgrid structured electric vehicle charging station and its energy management approach," *Energies*, vol. 12, no. 1, p. 168, Jan. 2019.

[9] L. Shen, Q. Cheng, Y. Cheng, L. Wei, and Y. Wang, "Hierarchical control of DC micro-grid for photovoltaic EV charging station based on flywheel and battery energy storage system," *Electr. Power Syst. Res.*, vol. 179, Feb. 2020, Art. no. 106079.

[10] L. Yao, Z. Damiran, and W. H. Lim, "Optimal charging and discharging scheduling for electric vehicles in a parking station with photovoltaic system and energy storage system," *Energies*, vol. 10, no. 4, p. 550, Apr. 2017.

[11] E. González-Rivera, R. Sarrias-Mena, P. García-Triviño, and L. M. Fernández-Ramírez, "Predictive energy management for a wind turbine with hybrid energy storage system," *Int. J. Energy Res.*, vol. 44, no. 3, pp. 2316–2331, Mar. 2020.

[12] Y. Zheng, Y. Song, D. J. Hill, and K. Meng, "Online distributed MPC-based optimal scheduling for EV charging stations in distribution systems," *IEEE Trans. Ind. Informat.*, vol. 15, no. 2, pp. 638–649, Feb. 2019.

[13] H. Zheng, J. Wu, W. Wu, and Y. Wang, "Integrated motion and powertrain predictive control of intelligent fuel cell/battery hybrid vehicles," *IEEE Trans. Ind. Informat.*, vol. 16, no. 5, pp. 3397–3406, May 2020.

[14] J. Hu, Y. Shan, M. J. Guerrero, A. Ioinovici, K. W. Chand, and J. Rodriguez, "Model predictive control of microgrids—An overview," *Renew. Sustain. Energy Rev.*, vol. 136, Feb. 2021, Art. no. 110422.

[15] J. Rodriguez, R. Heydari, Z. Rafiee, H. A. Young, F. Flores-Bahamonde, and M. Shahparasti, "Model-free predictive current control of a voltage source inverter," *IEEE Access*, vol. 8, pp. 211104–211114, Dec. 2020.

[16] T. Chen, O. Abdel-Rahim, F. Peng, and H. Wang, "An improved finite control set-MPC-based power sharing control strategy for islanded AC microgrids," *IEEE Access*, vol. 8, pp. 52676–52686, Mar. 2020.

[17] M. Jayachandran and G. Ravi, "Predictive power management strategy for PV/battery hybrid unit based islanded AC microgrid," *Int. J. Electr. Power Energy Syst.*, vol. 110, pp. 487–496, Sep. 2019.

[18] H. H. Abdeltawab and Y. A.-R. I. Mohamed, "Market-oriented energy management of a hybrid wind-battery energy storage system via model predictive control with constraint optimizer," *IEEE Trans. Ind. Electron.*, vol. 62, no. 11, pp. 6658–6670, Nov. 2015.

[19] D. P. E. Silva, J. L. F. Salles, J. F. Fardin, and M. M. R. Pereira, "Management of an island and grid-connected microgrid using hybrid economic model predictive control with weather data," *Appl. Energy*, vol. 278, Nov. 2020, Art. no. 115581.

[20] U. R. Nair and R. Costa-Castello, "A model predictive control-based energy management scheme for hybrid storage system in islanded microgrids," *IEEE Access*, vol. 8, pp. 97809–97822, Jun. 2020.

[21] Y. Liu, H. Abu-Rub, B. Ge, F. Blaabjerg, O. Ellabban, and P. C. Loh, *Impedance Source Power Electronic Converters*. Hoboken, NJ, USA: Wiley, 2016.
[22] M. Shen, A. Joseph, J. Wang, F. Z. Peng, and D. J. Adams, "Comparison of traditional inverters and Z-source inverter for fuel cell vehicles," *IEEE Trans. Power Electron.*, vol. 22, no. 4, pp. 1453–1463, Jul. 2007.
[23] P. García-Triviño, J. P. Torreglosa, F. Jurado, and L. M. F. Ramírez, "Optimised operation of power sources of a PV/battery/hydrogen-powered hybrid charging station for electric and fuel cell vehicles," *IET Renew. Power Gener.*, vol. 13, no. 16, pp. 3022–3032, Dec. 2019.
[24] *Electric Vehicle Conductive Charging System—Part 1: General Requirements*, document IEC 61851-1:2010, 2016.
[25] G. Pasaoglu, D. Fiorello, L. Zani, A. Martino, A. Zubaryeva, and C. Thiel, "Projections for electric vehicle load profiles in Europe based on travel survey data contact information," JCR Sci. Policy Rep., Milan, Itally, Tech. Rep. EUR 25993, 2013.
[26] J. P. Torreglosa, P. García, L. M. Fernández, and F. Jurado, "Energy dispatching based on predictive controller of an off-grid wind turbine/photovoltaic/hydrogen/battery hybrid system," *Renew. Energy*, vol. 74, pp. 326–336, Feb. 2015.
[27] P. J. Corral-Vega, P. García-Triviño, and L. M. Fernández-Ramírez, "Design, modelling, control and techno-economic evaluation of a fuel cell/supercapacitors powered container crane," *Energy*, vol. 186, Nov. 2019, Art. no. 115863.
[28] L. Zhao, J. Brouwer, S. James, J. Siegler, E. Peterson, A. Kansal, and J. Liu, "Servers powered by a 10 kW in-rack proton exchange membrane fuel cell system," in *Proc. ASME 12th Int. Conf. Fuel Cell Sci., Eng. Technol.*, Boston, MA, USA, Jun./Jul. 2014, p. 8.
[29] ProtonOnsite. (2018). *C Series*. [Online]. Available: http://www.protononsite.com/sites/default/files/2017-07/PD-0600-0068-revF.pdf
[30] M. Ortega, M. V. Ortega, F. Jurado, J. Carpio, and D. Vera, "Bidirectional DC–DC converter with high gain based on impedance source," *IET Power Electron.*, vol. 12, no. 8, pp. 2069–2078, Jun. 2019.
[31] P. García, J. P. Torreglosa, L. M. Fernández, and F. Jurado, "Control strategies for high-power electric vehicles powered by hydrogen fuel cell, battery and supercapacitor," *Expert Syst. Appl.*, vol. 40, no. 12, pp. 4791–4804, 2013.
[32] HOPPECKE Batterien. (2017). *Sun Power VR L Series OPzV*. [Online]. Available: https://us.hoppecke.com/fileadmin/Redakteur/Hoppecke-
[33] Y. Liu, B. Ge, H. Abu-Rub, and F. Z. Peng, "Control system design of battery-assisted quasi-Z-source inverter for grid-tie photovoltaic power generation," *IEEE Trans. Sustain. Energy*, vol. 4, no. 4, pp. 994–1001, Oct. 2013.
[34] L. Xu, J. Li, J. Hua, X. Li, and M. Ouyang, "Optimal vehicle control strategy of a fuel cell/battery hybrid city bus," *Int. J. Hydrogen Energy*, vol. 34, no. 17, pp. 7323–7333, Sep. 2009.
[35] Atersa Grupo Elecnor. (2015). *Ultra Tolerancia Positiva Datasheet Placa Solar A-330M ATERSA ULTRA*. [Online]. Available: https://atersa.shop/panel-solar-a-330m-ultra
[36] R. Sarrias-Mena, L. M. Fernández-Ramírez, C. A. García-Vázquez, and F. Jurado, "Electrolyzer models for hydrogen production from wind energy systems," *Int. J. Hydrogen Energy*, vol. 40, no. 7, pp. 2927–2938, Feb. 2015.
[37] The Mathworks Inc. *Optimization Toolbox Documentation*. Accessed: Jul. 2, 2021. [Online]. Available: https://es.mathworks.com/help/optim/ug/linprog.html
[38] R. Halvgaard, "Model predictive control for smart energy systems," M.S. thesis, Dept. Appl. Math. Comput. Sci., Tech. Univ. Denmark, Kongens Lyngby, Denmark, 2014.
[39] The Mathworks Inc. *Model Predictive Control Toolbox Documentation*. Accessed: Jul. 2, 2021. [Online]. Available: https://es.mathworks.com/help/mpc/

ENRIQUE GONZÁLEZ-RIVERA was born in Los Barrios, Cádiz, Spain. He received the B.Sc. degree in electrical engineering and the M.Sc. degree in industrial engineering from the University of Cádiz, Cádiz, in 2015 and 2017, respectively. Since 2018, he has been a Research Fellow with the Research Group in Sustainable and Renewable Electrical Technologies, Department of Electrical Engineering, University of Cádiz. His current research interest includes energy management in hybrid systems.

PABLO GARCÍA-TRIVIÑO was born in La Línea de la Concepción, Cádiz, Spain, in 1984. He received the B.Sc. degree in electrical engineering, the M.Sc. degree in industrial engineering, and the Ph.D. degree from the University of Cádiz, Cádiz, in 2005, 2007, and 2010, respectively. Since 2008, he has been an Associate Professor with the Department of Electrical Engineering, University of Cádiz. His current research interests include power systems and power management in hybrid systems.

RAÚL SARRIAS-MENA was born in La Línea de la Concepción, Cádiz, Spain, in 1985. He received the M.Sc. degree in industrial engineering and the Ph.D. degree from the University of Cádiz, in 2010 and 2016, respectively. He is currently a Professor with the Engineering Department of Engineering in Automation, Electronics and Computer Architecture & Networks, University of Cádiz. His research interests include the study of strategies regulation and control applied to renewable hybrid systems and energy storage systems.

JUAN P. TORREGLOSA was born in Seville, Spain, in 1985. He received the M.Sc. degree in industrial engineering and the Ph.D. degree from the University of Jaén, Jaén, Spain, in 2009 and 2012, respectively. He was a Researcher in different projects with the University of Jaén, from 2009 to 2015. Since 2015, he has been an Assistant Professor with the Electrical Engineering Department, University of Huelva, Huelva, Spain. His current research interest includes energy management applied to hybrid systems composed of renewable energy sources.

FRANCISCO JURADO (Senior Member, IEEE) was born in Linares, Jaén, Spain. He received the M.Sc. and Dr.Ing. degrees from the National University of Distance Education, Madrid, Spain, in 1995 and 1999, respectively. Since 1985, he has been a Professor with the Department of Electrical Engineering, University of Jaén, Jaén. His current research interests include power systems, modeling, and renewable energy.

LUIS M. FERNÁNDEZ-RAMÍREZ (Senior Member, IEEE) was born in Los Barrios, Cádiz, Spain. He received the M.Sc. degree in electrical engineering from the University of Seville, Seville, Spain, in 1997, and the Ph.D. degree from the University of Cádiz, Cádiz, in 2004. From 1997 to 2000, he was with the Department of Development and Research, Desarrollos Eolicos S.A., Seville. In 2000, he joined the University of Cádiz, where he is currently an Associate Professor with the Department of Electrical Engineering and the Head of the Research Group in Sustainable and Renewable Electrical Technologies (PAIDI-TEP023). His research interests include smart grids, renewable energy, energy storage, hydrogen systems, and power converters and control.